Check for updates

Energy Technology
Generation, Conversion, Storage, Distribution
www.entechnol.de

Binder-Assisted Dispersion of Agglomerated Carbon Nanotubes for Efficiently Establishing Conductive Networks in Cathodes of Li-Ion Batteries

Mengxuan Zhang, Guoqing Ning, and Zhihua Xiao*

Carbon nanotubes (CNTs) are a promising conductive additive for Li-ion batteries. However, good dispersion of agglomerated CNTs (ACNTs) still remains challenge. Herein, a binder-assisted dispersion of ACNTs is demonstrated to efficiently construct a homogeneous conductive network in $LiFePO_4$ cathodes. The addition of polyvinylidene fluoride (PVDF) significantly reduces the size of ACNT agglomerates, which leads to better dispersion of ACNTs in *N*-methyl-pyrrolidone. The $LiFePO_4$ electrodes with conductive networks constructed from PVDF–ACNT suspensions exhibit superior electrode performance, as compared to those using the commercial CNT slurry.

For the demand of portable devices and electric vehicles, it is critical to develop Li-ion batteries (LIBs) with high energy density and good cycling stability.[1–3] The battery performance is affected not only by the intrinsic properties of active materials but also the electrode structure. Good contact between electrode and electrolyte and a well-dispersed conductive network are highly desired for fast Li ion diffusion and charge transfer.[4–6] Carbon nanotubes (CNTs) with high conductivity and robust linear morphology have been proved to be a superior conductive additive,[1,7–9] capable of achieving better electrode performance as compared to carbon black (CB) and carbon fibers.[10,11] However, the agglomeration of CNTs aroused due to their large length–diameter ratio has made it difficult to construct a homogeneous CNT network in electrodes.[12–14] Especially, the industrial-scale mass production of CNTs is mainly conducted in nanoagglomerate fluidization beds (NAFBs), from which agglomerated CNTs (ACNTs) with highly winding of CNTs are produced.[15] Recently, we found that vertically aligned CNTs have better dispersibility as compared to the ACNTs. Using the vertically aligned CNTs, a stable low concentration CNT suspension has been prepared for fabricating cathode with a well-dispersed conductive network.[15] However, the dispersion of ACNTs still remains a challenge. Considering that ACNTs have almost the largest production amount in industry, an efficient dispersion of ACNTs is highly desirable.

M. Zhang, Dr. G. Ning, Z. Xiao
State Key Laboratory of Heavy Oil Processing
China University of Petroleum
Beijing, Changping 102249, China
E-mail: ngq@cup.edu.cn

The ORCID identification number(s) for the author(s) of this article can be found under https://doi.org/10.1002/ente.202000589.

DOI: 10.1002/ente.202000589

The dispersion techniques of ACNTs include mechanical techniques like ultrasonification, ball milling, and functionalization techniques. Functionalization of CNTs includes covalent functionalization using strong acid to etch the surface of CNTs and physical functionalization which utilize polymers and surfactants (e.g., cetyl trimethyl ammonium bromide, dodecyl trimethyl ammonium bromides, and sodium dodecyl sulfate[16–19]) to change the interfacial properties of CNTs. In all the aforementioned techniques, the preparation of covalent functionalized CNTs is not environmentally friendly due to the use of strong acid. In contrast, physical functionalization has low cost and less damage, whereas it is difficult to obtain obvious enhancement in CNT dispersion. Although CNTs have been used as an additive to improve the conductivity and mechanical properties of polyvinylidene fluoride (PVDF),[20] no research has been focused on the use of PVDF to improve the dispersion of CNTs in a slurry. In this article, PVDF, a common binder in electrode, is adopted to assist the dispersion of ACNTs in *N*-methyl-pyrrolidone (NMP), for establishing an efficient conductive network in $LiFePO_4$ (LFP) cathodes. The addition of PVDF has significantly promoted the stability and viscosity of the ACNT suspension, which is in favor of relieving agglomeration of CNTs and consequently forming a well-dispersed conductive network in cathode. The as-obtained LFP cathode delivers remarkable rate capability, excellent cycling stability, and low temperature performance, obviously superior to the LFP cathode prepared by a traditional method. Considering that PVDF has been widely used in electrode fabrication, no harmful effect is expected for the current approach. Therefore, the binder-assisted dispersion of ACNTs is promising to be widely applied for electrode fabrication.

ACNTs were prepared in a NAFB using a $FeMo/Al_2O_3$ catalyst, as previously reported.[21,22] The as-prepared ACNT powder is composed of particles in size of several millimeters, showing the formation of agglomerates due to the fast growth of CNTs from a central catalyst particle with a mass increases more than 30 times. The primary agglomerates of CNTs are hard to disentangle even in a diluted ethanol suspension with the aid of long time ultrasonification (**Figure 1**a), probably due to the strong interaction between CNTs and catalyst cores (indicated by A) or the firm entangling between curled CNTs (indicated by B). The dispersibility of ACNTs in NMP was tested with a low CNT concentration (0.2 wt%). Optical microscopic observation (the inset of Figure 1b) shows that obvious agglomerates in size

MRD EX. 2009
LGES v MRD
IPR2024-01013

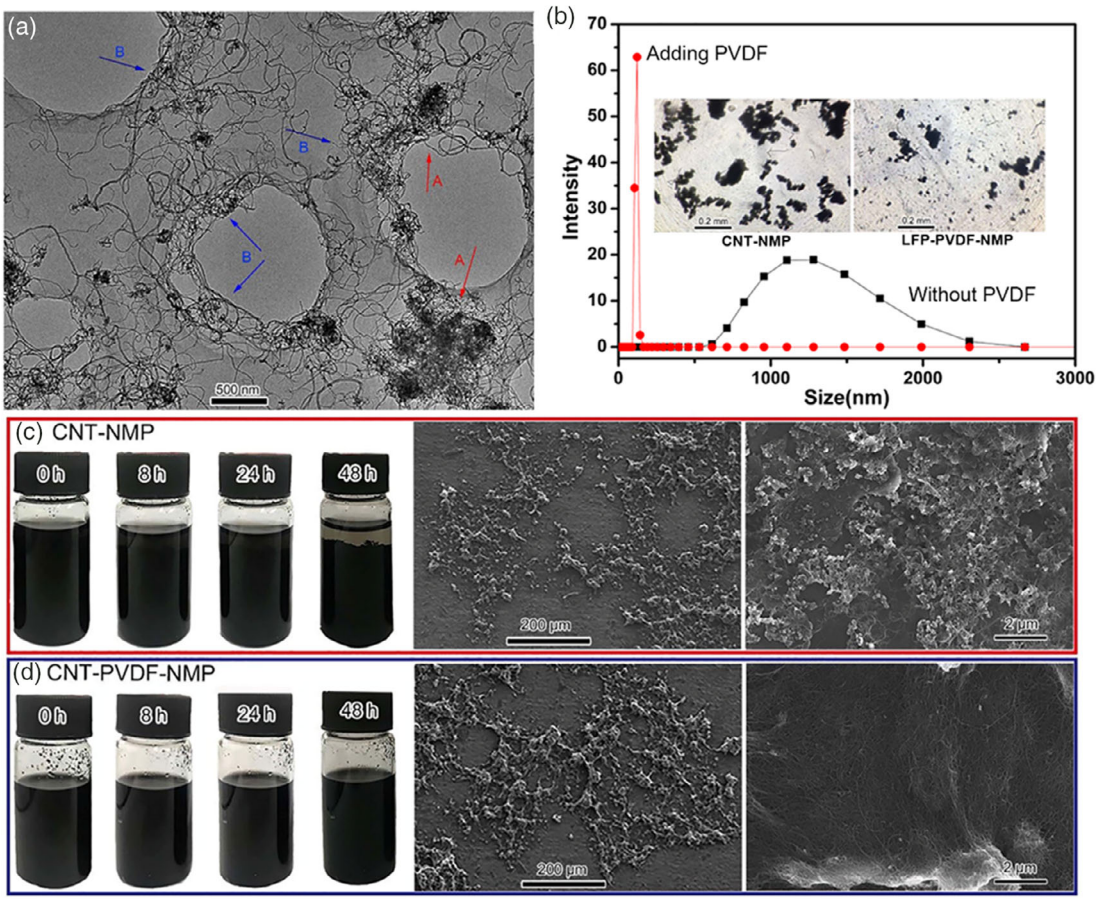

Figure 1. a) Transmission electron microscope image of ACNTs after dispersion in ethanol. b) Particle size distribution (derived by DLS analysis) of ACNTs dispersed in NMP with and without PVDF. The insets of (b) are optical microscopic photos of the CNT–NMP and CNT–PVDF–NMP suspensions. The stability and the SEM images of a c) dried drop of the CNT–NMP and d) CNT–PVDF–NMP suspensions.

of about 50 μm exist in the ACNT–NMP suspension after 10 min ultrasonification. In contrast, after adding PVDF (with a PVDF to CNTs mass ratio of 7:1), the CNT particle size in the suspension has been significantly reduced. Furthermore, dynamic light scattering (DLS) analysis was performed on a CNT–NMP suspension with or without adding PVDF. As shown in Figure1b, the particle size distribution after adding PVDF becomes sharper and moves to much smaller position as compared to the suspension without PVDF. It provides a strong evidence to prove that the addition of PVDF has decreased the size of CNT agglomerates and improved the dispersity of ACNTs. Both the optical microscopic observation and the DLS analysis show that adding PVDF has significantly improved the dispersion of ACNTs in NMP. It is noticeable that the introduction of PVDF in the ACNT suspension will not bring any harmful effects on the electrode performance since PVDF is a widely adopted binder in cathodes of LIBs.

As shown in Figure 1c, obvious sediments are observed in the CNT–NMP suspension after standing for 48 h. In contrast, the CNT–PVDF–NMP suspension keeps stable after 48 h (Figure 1d). It indicates that the addition of PVDF has significantly improved the dispersion stability of ACNTs in NMP. To get more information on the dispersed state of ACNTs in suspension, the initial suspension (after ultrasonification treatment) was dropped onto an aluminum foil set at an angle, and then characterized by scanning electron microscope (SEM) observation after drying. As shown in Figure 1c (right), CNT agglomerates with morphology similar to the original ACNTs are found in the sample prepared from the CNT–NMP suspension. In contrast, a network-like morphology is found in the sample prepared from the CNT–PVDF–NMP suspension (Figure 1d). In a closer view, one can see a dense CNT mat, without obvious agglomeration of CNTs. It implies that disentangling and redistribution of CNTs have occurred in the PVDF-added suspension, which might help to establish an evenly distributed CNT network in electrodes.

In a CNT–PVDF–NMP suspension, PVDF molecular chains would coat onto CNT surface due to the strong interaction between PVDF and CNTs.[23] As a result, the solid solution interaction between CNTs and the PVDF–NMP solution would be significantly promoted, as compared to that between CNTs and pure NMP. We further tested the viscosities of the CNT–PVDF–NMP suspensions. The suspension viscosity increases from 2 mPa s^{-1} for the CNT–NMP suspension without PVDF to 35 mPa s^{-1} after adding PVDF. The improvement of viscosity can increase the flowing shear force between CNTs and solvent, which is in favor of disentangling the CNT agglomerates during violent agitation

© 2020 Wiley-VCH GmbH

21944296, 2020, 12, Downloaded from https://onlinelibrary.wiley.com/doi/10.1002/ente.202000589 by Stephen Zinda , Wiley Online Library on [06/03/2025]. See the Terms and Conditions (https://onlinelibrary.wiley.com/terms-and-conditions) on Wiley Online Library for rules of use; OA articles are governed by the applicable Creative Commons License

or ultrasonification and consequently leading to a good dispersion of CNTs with enhanced stability.

The CNT–PVDF–NMP suspensions were used to construct a conductive network in LFP cathodes. In the LFP cathode without adding ACNTs (LFP–A0, **Figure 2**a), small CB particles are embedded in the LFP coating, and no CNTs exist. The LFP particles have smooth surfaces and a larger particle size than the CB particles, which makes it possible to distinguish LFP and CB particles by their morphologies, as indicated by the arrows in Figure 2a. In the LFP cathode fabricated with the CNT–NMP suspension (LFP–A1, Figure 2b), CNT agglomerates are clearly observed. The dispersion of CNTs is uneven in LFP–Al, probably due to the existence of CNT agglomerates in the CNT–NMP suspension. In contrast, no obvious CNT agglomerates are observed in a wide SEM view field for the LFP cathode fabricated with the CNT–PVDF–NMP suspension (LFP–A1–P7, Figure 2c,d). For LFP–A1–P7, A represents ACNTs, P represents PVDF, and the numbers 1 and 7 represent the ACNT to PVDF mass ratio of 1:7 in the CNT–PVDF–NMP suspension. SEM observation in wider view fields (Figure S1, Supporting Information) further confirms that the dispersion of CNTs in LFP–A1–P7 is much better than that in LFP–A1. It indicates that more even distribution of ACNTs in electrode is realized due to the PVDF-assisted predispersion of ACNTs in NMP.

The electrode performances of the as-prepared electrodes are shown in **Figure 3**. As shown in Figure 3a, the average specific capacities of LFP–A1–P7 are 159.7, 157.3, 152.8, 147.0, and 133.2 mAh g^{-1} at 0.2, 0.5, 1, 2, and 5 C, respectively, significantly higher than those of LFP–A1. It indicates that the addition of PVDF in ACNT suspension has efficiently enhanced the rate capability of LFP electrode due to the better dispersion of ACNTs in electrode. The capacity retention of LFP–A1–P7 at 5 C is 83.4%, obviously higher than that of LFP–A1 (79.8%), as shown in Figure S2, Supporting Information. Figure 3b shows the charge/discharge curves at 5 C for the LFP electrodes. Compared to LFP–A1, the discharge capacity of LFP–A1–P7 is extended at the 3.3 V platform, implying that more LFP particles are involved in energy storage due to the good connection by ACNTs. The cycling performances at 1 C are shown in Figure 3c. Compared to LFP–A1, LFP–A1–P7 exhibits higher discharge capacity (151.0 mAh g^{-1} in average) and similar capacity retention (90% after 100 cycles). In the electrochemical impedance spectroscopy (EIS) plots (Figure 3d), the semicircle diameter of LFP–A1–P7 at high frequency, corresponding to the charge transfer resistance, is smaller than that of LFP–A1. The higher conductivity of LFP–A1–P7 can be attributed to the well-dispersed conductive network in electrode, which has been established via the PVDF-assisted predispersion of ACNTs.

We further tested the electrodes with higher LFP content. In these electrodes, the mass ratio of LFP, PVDF, ACNTs, and CB is 94:2.5:1:2.5. The electrode LFP94–A1–P2.5 was prepared using a CNT–PVDF–NMP suspension (CNT: PVDF = 1:2.5). As a control sample, LFP94–A1 was prepared using a CNT–NMP suspension. Compared to LFP94–A1, LFP94–A1–P2.5 exhibits better rate capabilities and cycling performance (Figure S3, Supporting Information). It indicates that the addition of PVDF in ACNTs suspension works well to promote electrode performance at a higher LFP content.

Furthermore, the low temperature performances of the LFP electrodes were tested at −20 °C. The LFP cathode fabricated with a commercial CNT–NMP slurry (LFP–A1–C) is used as a control sample. As shown in **Figure 4**a, the average specific capacity at 0.2

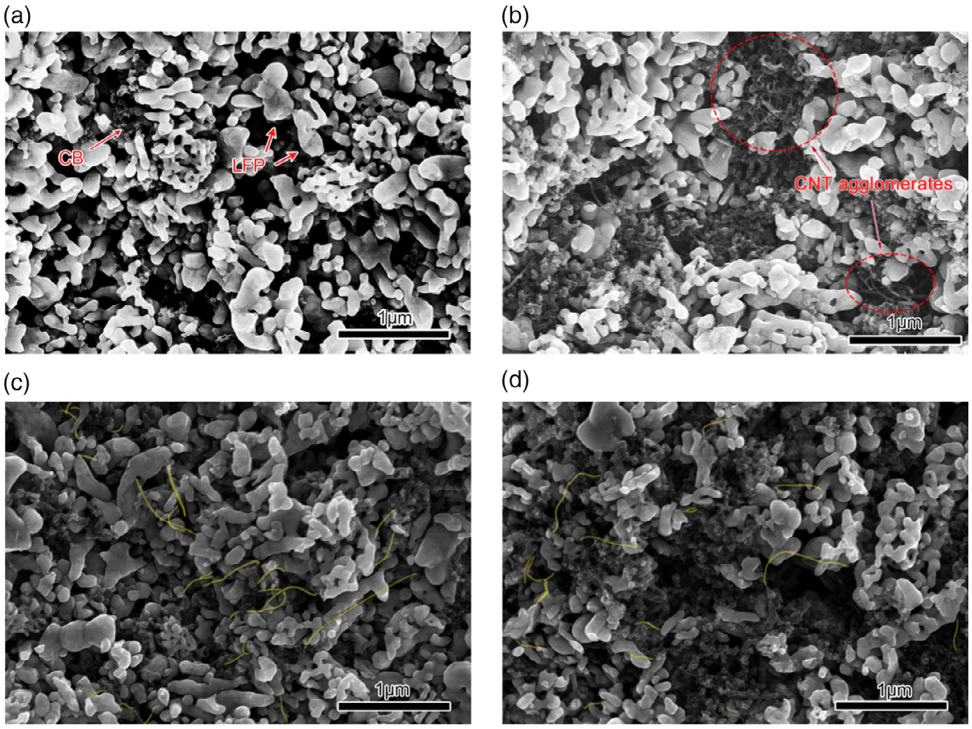

Figure 2. a) SEM image of LFP–A0 , b) LFP–A1, and c,d) LFP–A1–P7.

 © 2020 Wiley-VCH GmbH

21944296, 2020, 12, Downloaded from https://onlinelibrary.wiley.com/doi/10.1002/ente.202000589 by Stephen Zinda , Wiley Online Library on [06/03/2025]. See the Terms and Conditions (https://onlinelibrary.wiley.com/terms-and-conditions) on Wiley Online Library for rules of use; OA articles are governed by the applicable Creative Commons License

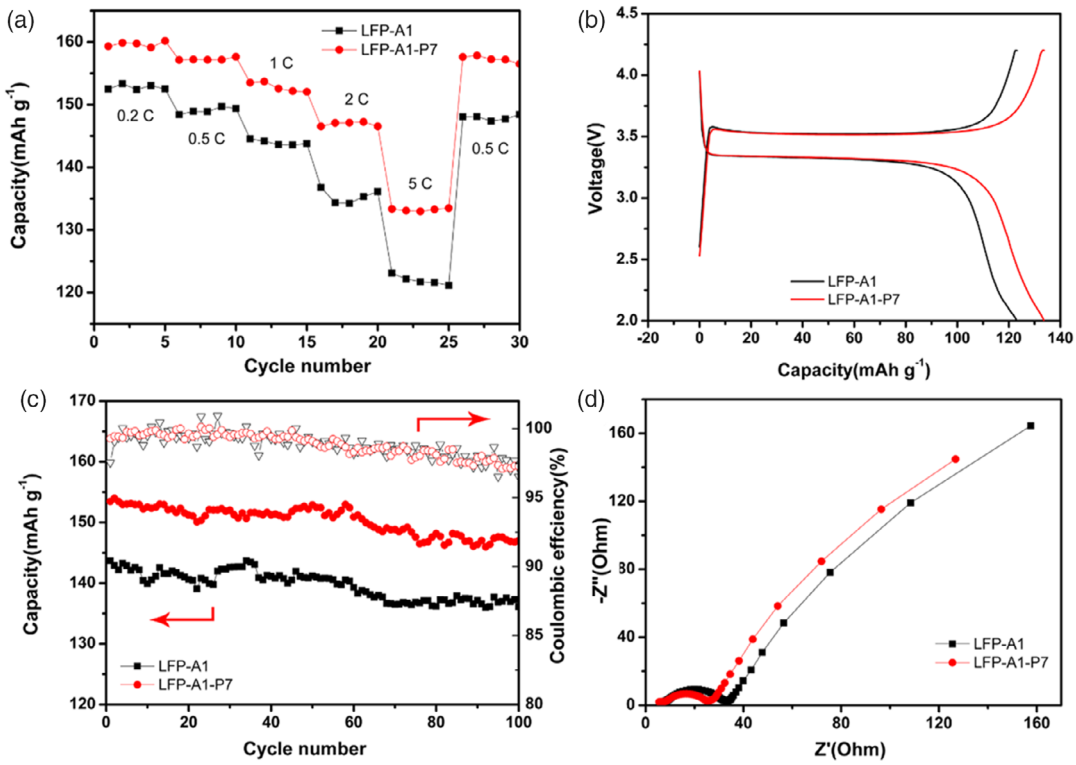

Figure 3. a) Rate capabilities, b) charge–discharge curves at 5 C, c) cycling performance and Coulombic efficiency at 1 C, and d) impedance curves of LFP–A1, LFP–A1–P7 at normal temperature.

C for LFP–A1–P7 is 140 mAh g^{-1} at −20 °C, 12.7% lower than that at room temperature (160.4 mAh g^{-1}). LFP–A1–P7 exhibits superior rate capability at low temperature, as compared to LFP–A1 and LFP–A1–C. In the charge–discharge curves at 0.5 C (Figure 4b), the charge and discharge voltage platforms for LFP–A1–P7 appear at 3.5 and 3.3 V, respectively. However, an obvious discharge voltage drop from 3.3 to 3.1 V is observed for LFP–A1–C. Similar voltage drop is also found for LFP–A1–C at 2 C (Figure 4c) and 5 C (Figure 4d), and the platform at lower voltage is continuously extended as the charge–discharge rate increases. At 5 C, LFP–A1 also exhibits a voltage drop in the discharge curve (Figure 4d). We label the platform at higher voltage as Stage I, and that at lower voltage as Stage II. Considering that the polarization resistance would increase at a higher rate, the appearance of Stage II indicates the existence of a zone with worse CNT contact. Thus, we speculate that the electrode can be divided into two zones: the CNT–CB-covered zone and the CB-only zone, as shown in the inset of Figure 4e. The solid chilling shrink in the CB-only zone would lead to a weakened contact between LFP and CB particles, thus resulting in an increased contact resistance and leading to a lower output voltage. CNTs are capable of providing a long-range conducting network with high stability even at low temperature. Therefore, the contact resistance in the CNT–CB-covered zone will not be lowered as the temperature drops, thus remaining at a higher output voltage. We calculate the CNT coverage (X) by the following equation

$$X = C_{\mathrm{I}}/(C_{\mathrm{I}} + C_{\mathrm{II}}) \quad (1)$$

where C_{I} represents the specific capacity in Stage I, and C_{II} represents the specific capacity in Stage II. For LFP–A1–P7, all capacity is delivered in Stage I. It indicates that all electrode zones are well connected by the CNT conductive network due to the good dispersion of CNTs, corresponding to a CNT coverage of 100%. The CNT coverages for LFP–A1 and LFP–A1–C are 85% and 65%, respectively (Figure 4e), aroused by the fact that some areas are not covered by ACNTs network due to their inhomogeneous dispersion. Figure 4f shows the Nyquist plots of the as-prepared electrodes in the frequency range of from 0.01 Hz to 100 kHz. In the impedance patterns, the width of the semicircle at the high frequency zone corresponds to the charge transfer resistance. Among the three electrodes, LFP–A1–P7 exhibits the lowest charge transfer resistance. It can be attributed to the good dispersion of ACNTs with a CNT coverage of 100%. Compared to LFP–A1–C, LFP–A1 has a lower charge transfer resistance. It implies that the addition of ACNTs via a low concentration CNT suspension is superior to the operation using a dense ACNT slurry, for obtaining a good dispersion of ACNTs in electrode.

The commercial CNT slurry is a pasty fluid due to the high CNT content (5 wt%). In the slurry, the distance between CNTs is too close to avoid the contact between CNTs. Therefore, the commercial CNT slurry is likely composed of CNT agglomerates absorbing NMP, rather than individual CNTs dispersed in NMP. Once the commercial CNT slurry is directly mixed with LFP and PVDF, there is no chance to disentangle CNT agglomerates, thus leading to an uneven CNT distribution in the final electrode. In contrast, the CNT content in the CNT–PVDF–NMP suspension

© 2020 Wiley-VCH GmbH

21944296, 2020, 12, Downloaded from https://onlinelibrary.wiley.com/doi/10.1002/ente.202000589 by Stephen Zinda , Wiley Online Library on [06/03/2025]. See the Terms and Conditions (https://onlinelibrary.wiley.com/terms-and-conditions) on Wiley Online Library for rules of use; OA articles are governed by the applicable Creative Commons License

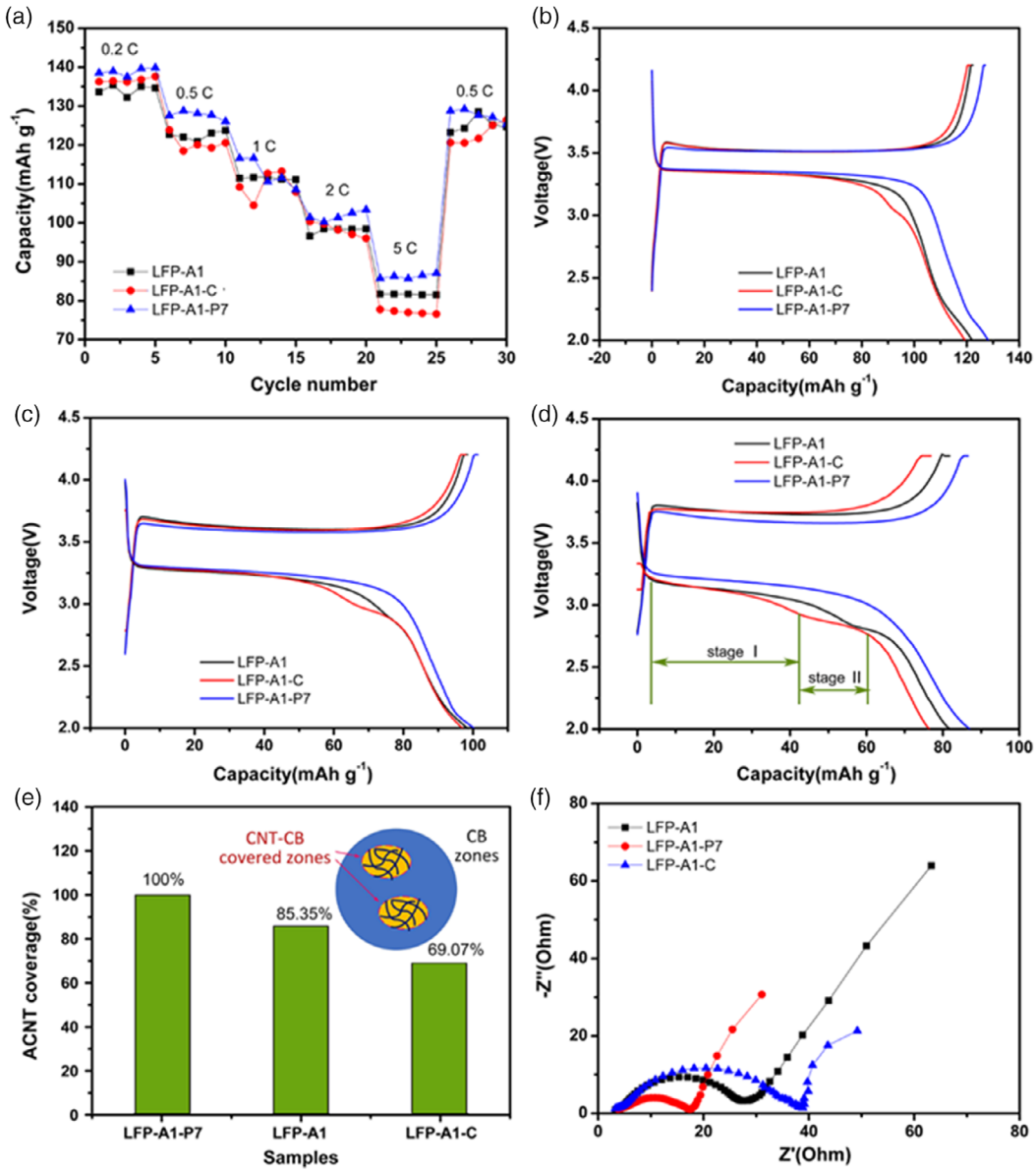

Figure 4. Low temperature (−20 °C) electrode performances of the as-prepared electrodes: a) rate capabilities and charge–discharge curves at b) 0.5 C, c) 2 C, and d) 5 C. e) The ACNT coverage ratio and f) impedance curves of the electrodes. The inset of (e) is the figure showing the different zones in an electrode with or without CNT covering.

is only 0.2 wt%. The small CNT content is capable of reducing the possibility of CNT retangling. As a result, the CNTs predispersed in NMP with the aid of PVDF have constructed a better conductive network in electrodes and lead to better electrochemical performance.

The effect of the PVDF content in the CNT–PVDF–NMP suspension is further investigated. The LFP electrodes are labeled as LFP–A1–Px in which x represents the mass ratio of PVDF to ACNTs in the CNT–PVDF–NMP suspensions. As shown in **Figure 5**a, the discharge capacities are gradually improved as the PVDF amount in the CNT–PVDF–NMP suspension increases, and the specific capacity of LFP–A1–P7 is the highest. It provides another evidence showing that the addition of PVDF in the ACNT suspension has efficiently promoted the CNT dispersion in electrode. The charge–discharge curves of LFP electrodes at 5 C are shown in Figure 5b. The discharge platform at 3.3 V is continuously extended as the PVDF amount in the CNT suspensions increases. It implies that more LFP particles have been involved in the charge–discharge processes due to the enhanced CNT covering. In the impedance curves (Figure 5c), the semicircle diameter, corresponding to the charge transfer resistance, decreases as the PVDF amount increases. It indicates that the PVDF-assisted ACNT dispersion has efficiently reduced the charge transfer resistance for LFP electrodes.

As shown in Figure 5, LFP–A1–P7 exhibits the best electrode performance. It implies that the dispersion of ACNTs has been

© 2020 Wiley-VCH GmbH

21944296, 2020, 12, Downloaded from https://onlinelibrary.wiley.com/doi/10.1002/ente.202000589 by Stephen Zinda , Wiley Online Library on [06/03/2025]. See the Terms and Conditions (https://onlinelibrary.wiley.com/terms-and-conditions) on Wiley Online Library for rules of use; OA articles are governed by the applicable Creative Commons License

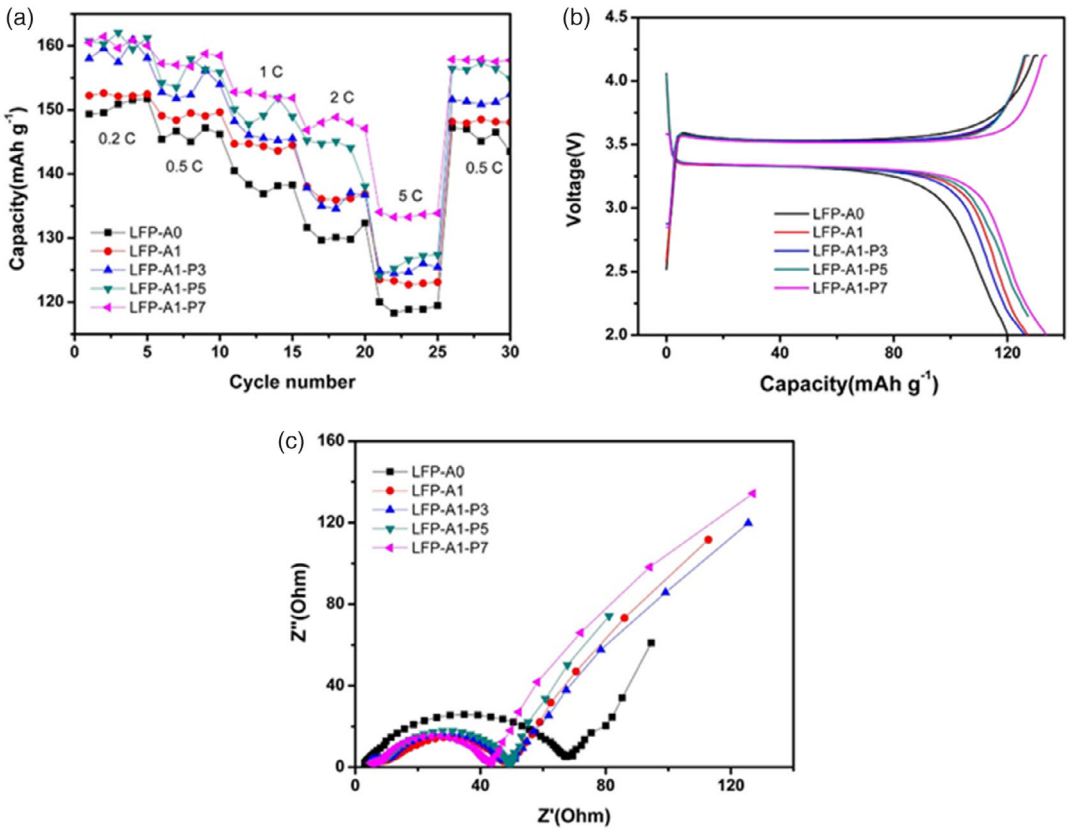

Figure 5. a) Rate capacities, b) charge–discharge curves at 5 C, and c) impedance curves of the electrodes prepared with different PVDF amounts in the ACNT suspensions.

continuously promoted as the PVDF to CNT ratio in the CNT–PVDF–NMP suspension increases from 0 to 7. Because the final PVDF to CNT ratio in electrodes is 7, further increase in the PVDF content will change the electrode composition. Therefore, we conclude that at a CNT content of 1 wt% and a PVDF content less than 7 wt% (in the final electrode), the larger amount of PVDF addition in CNT suspension always promotes the dispersion of ACNTs.

Furthermore, we tested a higher CNT content (2 wt%). The mass ratio of LFP, PVDF, CB, and ACNTs was set as 91:5:2:2. As shown in Figure S4, Supporting Information, LFP91–A2–P3 displays the highest discharge capacities. It indicates that the dispersion of ACNTs has been continuously enhanced as the PVDF to CNT ratio in CNT suspension increases from 0 to 3:2. When the PVDF to CNT ratio further increases to 5:2 (LFP91–A2–P5), the discharge capacity shows a distinct decline. It implies that at a higher CNT content, an excessive addition of PVDF might increase the adhesive force between CNTs and is unfavorable for good CNT dispersion.

In summary, the addition of PVDF in ACNT suspension has significantly improved the stability and dispersibility of ACNTs. A well-dispersed CNT conductive network in LFP electrodes is successfully constructed using the binder-added ACNT suspension. The good dispersion of ACNTs in electrode has resulted in a low charge transfer resistance and significantly enhanced electrode performance. Especially, the LFP electrode with PVDF-assisted dispersion of ACNTs exhibits superior rate capacities and stable discharge platform at −20 °C. Our result provides a simple approach to disperse the highly entangling ACNTs, and is promising to be commercially applied for promoting the electrode performance of LIBs.

Experimental Section

Preparation of CNT–PVDF–NMP Suspension: First, PVDF was dispersed in NMP to form a homogeneous solution with a concentration of 7 wt%. Then, the PVDF solution (containing 70 mg of PVDF) and ACNTs (10 mg) were dispersed into NMP (3.92 g) in sequence with the aid of ultrasonification (JARCON PS10AD, 80 W) for an hour, resulting in an even CNT–PVDF–NMP suspension with a viscosity of 30 mPa·s^{-1}. The CNT concentration in the suspension was 0.2 wt%, and the CNT to PVDF mass ratio was 1:7.

Materials Characterization: The dispersion state of these suspensions was characterized by optional microscope (phoenix BMC500-DB500U-ICCF) and SEM (SEM, SU8010). The viscosity of the suspensions was characterized by Viscosimeter (LICHEN, NDJ-1). The particle size distribution of CNTs in suspension with or without PVDF was characterized by a dynamic light scatterometer (Malvern Mastersizer 2000).

Fabrication of LFP Cathodes: The CNT–PVDF–NMP suspensions were used to construct a conductive network in LFP (Tianjin Lishen Ltd. Co.500 nm) cathodes. The mass ratio of LFP, PVDF, CB, and ACNTs in the cathodes was set as 89:7:3:1. The LFP electrode was labeled as LFP–A1–P*x*, where A represented ACNTs, P represented PVDF, and *x* represented the PVDF to CNT mass ratio in the CNT–PVDF–NMP

 © 2020 Wiley-VCH GmbH

21944296, 2020, 12, Downloaded from https://onlinelibrary.wiley.com/doi/10.1002/ente.202000589 by Stephen Zinda , Wiley Online Library on [06/03/2025]. See the Terms and Conditions (https://onlinelibrary.wiley.com/terms-and-conditions) on Wiley Online Library for rules of use; OA articles are governed by the applicable Creative Commons License

suspension. It was noted that the PVDF content in different electrodes (LFP–A1–P*x*) was the same with each other, and the insufficient amount of PVDF had been complemented into the cathode slurry using high concentration PVDF solution.

To prepare the LFP–A1–P7 electrode (as an example), LFP (0.35 g), CB (11.8 mg), the CNT–PVDF–NMP suspension (1.97 g), and a small amount of NMP were mixed and magnetically stirred for 12 h to obtain a cathode slurry. The as-obtained slurry was uniformly coated onto an aluminum foil and dried. The resulted foil was cut into 13 mm discs and pressed at 4 MPa. The loading of LFP in the electrode was $\approx$2 mg cm^{-2}. Coin-type half cells were assembled in an argon-filled glove box using Li foils as counter electrode. The control LFP electrode prepared by the similar process except using a CNT–NMP suspension was labeled as LFP–A1. For preparing the slurry, the PVDF solution (7 wt% PVDF), the ACNT–NMP suspension (without PVDF), and LFP were mixed in a beaker under electromagnetic stirring for 12 h. The control LFP electrode prepared with a commercial CNT–NMP slurry as conductive additive was labeled as LFP–A1–C. The commercial CNT slurry (Jiangsu CNano Technology Co., Ltd. LB260-32) was composed of 5 wt% CNTs, 1 wt% dispersant, and 94 wt% NMP. In the fabrication of LFP–A1–C, the PVDF solution (7 wt% PVDF), the commercial CNT–NMP slurry (5 wt% CNT), LFP, and a small amount of NMP were mixed directly. The PVDF content in LFP–A1–C was 7 wt%, which was same with other electrodes. The control LFP electrode without adding ACNTs was labeled as LFP–A0 (LFP:PVDF:CB = 89:7:4, mass ratio).

Electrochemical Tests: The electrode performances of the as-prepared electrodes were tested on a Neware BTS3000 battery tester at different current densities in a voltage range of 2.5–4.2 V. EIS was tested on an electrochemical workstation (Zahner Zennium E) from 0.01 to 100 kHz.

Supporting Information

Supporting Information is available from the Wiley Online Library or from the author.

Acknowledgements

M.Z. and G.N. contributed equally to this work. This work was supported by the National Natural Science Foundation of China (No. 21776309).

Conflict of Interest

The authors declare no conflict of interest.

Keywords

carbon nanotubes, conductive additives, lithium-ion batteries

Received: June 24, 2020
Revised: September 30, 2020
Published online: October 20, 2020

[1] X. M. Liu, Z. D. Huang, S. W. Oh, B. Zhang, P. C. Ma, M. M. F. Yuen, J. K. Kim, *Composit. Sci. Technol.* **2012**, *72*, 121.
[2] M. Armand, J.-M. Tarascon, *Nature* **2008**, *7179*.
[3] X. L. Wu, Y. G. Guo, J. Su, J. W. Xiong, Y. L. Zhang, L. J. Wan, *Adv. Energy Mater.* **2013**, *3*, 1155.
[4] Y. Cai, D. Huang, Z. Ma, H. Wang, Y. Huang, X. Wu, Q. Li, *Electrochim. Acta* **2019**, *305*, 563.
[5] X. Wang, K. Wen, T. Chen, S. Chen, S. Zhang, *Appl. Surface Sci.* **2020**, *522*, 146507.
[6] F. Zhou, K. Qiu, G. Peng, L. Xia, *Electrochim. Acta* **2015**, *151*, 16.
[7] G. Wang, Q. Zhang, Z. Yu, M. Z. Qu, *Solid State Ion.* **2008**, *179*, 263.
[8] F. Napolskiy, M. Avdeev, M. Yerdauletov, O. Ivankov, S. Bocharova, S. Ryzhenkova, B. Kaparova, K. Mironovich, D. Burlyaev, V. Krivchenko, *Batteries* **2020**, *8*, 2000146.
[9] J.-K. Yoo, Y. Oh, T. Park, K. E. Lee, M.-K. Um, J.-W. Yi, *Batteries* **2019**, *7*, 1800845.
[10] X. Li, F. Kang, X. Bai, W. Shen, *Electrochem. Commun.* **2007**, *9*, 663.
[11] W. Guoping, Z. Qingtang, Y. Zuolong, *Solid State Ion.* **2008**, *179*, 263.
[12] P. He, J. Lian, D. Shi, L. Wang, W. J. Van Ooij, D. Mast, W. Li, Z. F. Ren, *MRS Proc.* **2003**, *791*.
[13] R. I. Rubel, M. H. Ali, M. A. Jafor, M. M. Alam, *AIMS Mater. Sci.* **2019**, *6*, 756.
[14] T. Tarlton, E. Sullivan, J. Brown, P. A. Derosa, *J. Appl. Phys.* **2017**, *121*, 085103.
[15] G. Ning, S. Zhang, Z. Xiao, H. Wang, X. Ma, *Carbon* **2018**, *132*, 323.
[16] J. Rausch, R.-C. Zhuang, E. Mäder, *Composit. A: Appl. Sci. Manufact.* **2010**, *41*, 1038.
[17] S. Javadian, A. Motaee, M. Sharifi, H. Aghdastinat, F. Taghavi, *Colloids Surf. A: Physicochem. Eng. Aspects* **2017**, *531*, 141.
[18] Y. Bai, J. Gao, C. Wang, R. Zhang, W. Ma, *J. Nanosci. Nanotechnol.* **2016**, *16*, 2239.
[19] I. Madni, C.-Y. Hwang, S.-D. Park, Y.-H. Choa, H.-T. Kim, *Colloids Surf. A: Physicochem. Eng. Aspects* **2010**, *358*, 101.
[20] S. Mishra, K. T. Kumaran, R. Sivakumaran, S. P. Pandian, S. Kundu, *Colloids Surf. A: Physicochem. Eng. Aspects* **2016**, *509*, 684.
[21] Y. Hao, Z. Qunfeng, W. Fei, Q. Weizhong, L. Guohua, *Carbon* **2003**, *41*, 2855.
[22] W. Qian, H. Yu, F. Wei, Q. Zhang, Z. Wang, *Carbon* **2002**, *40*, 2968.
[23] D. J. Welsh, L. J. O'Driscoll, S. W. D. Bailey, D. Visontai, K. Howes, H. Frampton, M. R. Bryce, C. J. Lambert, *RSC Adv.* **2015**, *5*, 95360.

© 2020 Wiley-VCH GmbH

21944296, 2020, 12, Downloaded from https://onlinelibrary.wiley.com/doi/10.1002/ente.202000589 by Stephen Zinda , Wiley Online Library on [06/03/2025]. See the Terms and Conditions (https://onlinelibrary.wiley.com/terms-and-conditions) on Wiley Online Library for rules of use; OA articles are governed by the applicable Creative Commons License